Article

Case Study on the Performance of High-Flowing Steel-Fiber-Reinforced Mixed-Sand Concrete

Haibin Geng [1], Yanyan Zhang [2,*], Huijuan Wang [3], Hao Zhong [1], Changyong Li [1,*] and Fenglan Li [1,3]

1   Collaborative Innovation Center for Efficient Utilization of Water Resources, North China University of Water Resources and Electric Power, Zhengzhou 450045, China; hbgeng@stu.ncwu.edu.cn (H.G.); zhonghao20001222@stu.ncwu.edu.cn (H.Z.); lifl64@ncwu.edu.cn (F.L.)
2   School of Building Engineering, Zhengzhou Business University, Zhengzhou 451200, China
3   Low-Carbon Eco-Building Materials Technology Innovation Center of Xuchang City, Zhongyuan Institute of Science and Technology, Zhengzhou 450046, China; wanghuijuan1@zykjxy.wecom.work
*   Correspondence: zhangyan2115@126.com (Y.Z.); lichang@ncwu.edu.cn (C.L.)

Abstract: To promote the efficient utilization of bulk solid wastes, including superfine river sand and fly ash, high-flowing steel-fiber-reinforced mixed-sand concrete (SFRMC) was developed in this study. Superfine river sand and coarse manufactured sand were mixed in a proportion of 4:6 to make the mixed sand. Fly ash, with a content of 30~75%, was blended with 0~12% silica fume on the premise of equivalent activity. The water dosage and sand ratio were adjusted with the volume fraction of steel fiber, which varied from 0.4 to 1.6%, to ensure the high flowability of fresh SFRMC. The mechanical properties, including cubic and axial compressive strengths, modulus of elasticity, splitting tensile strength, and flexural strength and toughness of the SFRMC, were analyzed, accounting for the influences of the contents of fly ash and steel fiber. The predictive formulas for the splitting tensile strength, modulus of elasticity, and flexural strength were proposed by introducing the influencing factors of steel fiber. The SFRMC showed an increased modulus of elasticity with increases in the steel fiber factor, and flexural toughness was enhanced with increased contents of both steel fiber and fly ash.

Keywords: steel-fiber-reinforced mixed-sand concrete; high flowability; mixed sand; fly ash; steel fiber; mechanical property

1. Introduction

Nowadays, the efficient utilization of bulk solid wastes has become a route to produce low-carbon concrete, which plays an important role in ecological environment protection. This promotes the production of concrete using recycled solid wastes, including recycled aggregate from waste concrete, plastic and rubber, mine tailings, and tunnel slags, as well as mineral admixtures, including fly ash, silica fume, ground granulated blast furnace slag, steel slag powder, ground granulated electric furnace phosphorous slag powder, and ground limestone [1–4]. Facing the exhausted status of natural sand due to the protection of riverbeds and farmlands, manufactured sand made of waste stones and gravel has become the main sand source for market supply [5,6]. However, from the perspective of production efficiency aspects, such as reducing costs, controlling the stone powder content, and avoiding secondary environmental pollution, manufactured sand is more likely to be made into coarse sand [7,8]. This raises a problem, as coarse manufactured sand is inadaptable to concrete production due to its poor workability and higher permeability [8–10], while another issue may arise from the quality control of concrete properties [11,12]. These deficiencies need to be offset using sufficient binder paste with a higher sand ratio.

On the other hand, the abundant superfine river sand (SRS) found along most river beaches is a potential risk to the environment, leaving the ground with less vegetational cover, especially in dry and windy seasons [13–15]. Compared with different treatment

methods, the low cost of SRS has led to its extensive utilization in modifying coarse sand to the required gradation and fineness of sand for concrete [16,17]. The advantage of SRS is that it has smooth and rounded grains to fill the gaps among coarse sand particles, resulting in an increase in the lubrication layer of mortar with the rolling effect of SRS to improve the flowability of fresh concrete. At the same time, the shortage of coarse manufactured sand can be made up with SRS [18–20]. This supports the engineering of mixed sand by compositing SRS and coarse manufactured sand for concrete production.

Meanwhile, as a commonly used mineral admixture of concrete, fly ash is limited to lower contents to avoid the drawback of decreased strength, especially at the early ages of the concrete [21,22]. As specified by China codes JGJ 52 [23] and GB/T 50146 [24], the fly ash content of concrete for reinforced concrete structures is less than 30–35% of the total mass of binders accompanying common Portland cement, whereas the fly ash content for prestressed concrete structures should be reduced by 10–15% for the same conditions as reinforced concrete structures. A study [20] on mixed-sand concrete with 30% fly ash content showed that it had high pumpability and could be prepared as per China codes JGJ52 [23] and JGJ 55 [25], and it had adaptable mechanical properties that could be predicted with the specifications of China code GB 50010 [26]. Since then, many studies have explored approaches to producing concrete with high contents of fly ash by compounding other high-activity admixtures, including silica fume, nano-silica, nano-$CaCO_3$, and metakaolin [27–30]. The aim is to accelerate the hydration of both fly ash and cement and enhance the positive effects of fly ash on the refinement of pores and improvements in the microstructure and interfacial transition zones [29,31]. A study by Choi et al. [32] indicated that by admixing superplasticizer and an air-entraining agent with a decreased water dosage and increased content of binders, a high-fluidity concrete with 50% fly ash content ensured early strength and reached the target strength at a curing age of 28 days. Yu et al. [33] reported that by lowering the water-to-binder ratio and properly combining raw materials, concrete with 40–70% fly ash content had adequate strength and workability, and the mechanical properties could be improved by admixing a small amount of silica fume. In general, high contents of fly ash can be used in concrete production with the help of high-activity admixtures in the proper mix proportions.

It is well known that steel fibers can reinforce mechanical properties, especially the tensile performance of concrete [34,35]. Contrary to other constituents of concrete, steel fibers are needle-like materials distributed in the concrete matrix, which leads to the concern that the reinforcement effect is related to the distribution and orientation of steel fibers in the concrete matrix. Therefore, the problem becomes complex, as there are many influencing factors, including the mix proportion, compaction method, and the steel fiber itself [34–36]. Therefore, the optimization of the mix proportion of steel-fiber-reinforced concrete plays an important role in the high performance of steel-fiber-reinforced concrete [37]. To maintain the equivalent workability of steel-fiber-reinforced concrete with an increase in steel fiber content, the water dosage and sand ratio need to increase in the mix proportion, and the absolute volume method is used due to the obviously different unit weight of steel-fiber-reinforced concrete [38]. Due to the bond of steel fibers to the concrete matrix, which markedly affects the strength of the mortar, the constituents of the mortar, including mineral admixtures and sand, behave as an inherent function that influences the reinforcement effect of steel fibers [39]. Thus, the reinforcement of steel fibers in mixed-sand concrete should be understood before its application.

Therefore, the mixed sand used for the development of high-flowing steel-fiber-reinforced mixed-sand concrete (SFRMC) is still a new area that should be deeply investigated. To access the economic benefits from the effective utilization of mixed sand, fly ash, and steel fibers, the function of each factor and their coupling actions were studied in this work. The fly ash content varied from 30% to 75% in the mass of total binders, and the volume fraction of steel fibers changed from 0.4% to 1.6%. Based on a previous study of mixed-sand concrete [20], the mixed sand was blended with 40% SRS and 60% manufactured sand, the sand ratio for concrete was 45%, and the water-to-binder ratio

was 0.36. Silica fume was added to keep equivalent activities of mineral admixtures with varying contents of fly ash and silica fume. The water dosage and the sand ratio of SFRMC were adjusted in relation to the volume fraction of steel fiber, and the dosages of other constituents were determined from the absolute volume method considering an equivalent mass of coarse aggregate replaced by steel fibers [38,40]. The workability of fresh SFRMC was determined with indices including the slump flowability, the static segregation rate, the pressure bleeding rate, and the air content, while the rheological properties were measured with indices of the yield stress and the plastic viscosity. Relationships between different mechanical properties are discussed based on the test results of cubic and axial compressive strengths, the modulus of elasticity, splitting tensile strength, and flexural strength and toughness.

2. Materials and Methods

2.1. Raw Materials

Except for silica fume, the raw materials were the same as those used for pumping mixed-sand concrete [20], which included ordinary Portland cement of 42.5 strength grade, class-II fly ash, crushed limestone in a continuous gradation of 5–20 mm particles, and mixed sand with 40% SRS and 60% manufactured sand. The properties and chemical compositions of silica fume are summarized in Tables 1 and 2, which met the specification of GB/T 27690 [41].

Table 1. Physical properties of silica fume.

Admixture	Apparent Density (kg/m^3)	Water Demand (%)	Water Content (%)	Activity Index (%)
Silica fume	2160	103.6	0.43	113.2

Table 2. Chemical compositions of silica fume.

Binder	Chemical Composites (%)						
	CaO	MgO	Al$_2$O$_3$	Fe$_2$O$_3$	SiO$_2$	SO$_3$	LOI
Silica fume	0.56	0.30	0.80	0.60	92.82	0.90	0.0675

Ingot mill steel fibers were used with a length l_f = 32.5 mm, an equivalent diameter d_f = 0.8 mm, and a tensile strength of 860 MPa. The additive was the polycarboxylate superplasticizer with a water reduction rate of 25%. The mix water was the tap water in Zhengzhou, China.

2.2. Mix Proportions and Preparation of SFRMC

The mix proportions of SFRMC were designed by the absolute volume method [38]. The mix design was based on a previous study of mixed-sand concrete with a target cubic compressive strength of 48.2 MPa at a strength grade of C40 [20], a fly ash content (β_{fa}) of 30%, a sand ratio ($\beta_{s,0}$) of 45%, a water-to-binder ratio of 0.36, a water dosage of 230 kg/m^3 aimed at obtaining a slump of (245 ± 15) m, a 25% water reduction with polycarboxylate superplasticizer, and a dosage of mix water $m_{w,0}$ = 172.5 kg/m^3.

For SFRMC with a varying volume fraction of steel fibers, the flowability of the fresh mix was ensured by adjusting the water dosage and the sand ratio with formulas as follows [38]:

$$m_{w,f} = (1 + 0.25\eta_f)m_{w,0} \tag{1}$$

$$\beta_{s,f} = (1 + 0.11\eta_f)\beta_{s,0} \tag{2}$$

$$\eta_f = \left(\frac{l_f}{d_f}\right)v_f\alpha_f \tag{3}$$

where $m_{w,f}$ is the water dosage of SFRMC; $m_{w,0}$ is the water dosage of referenced mixed-sand concrete; $\beta_{s,f}$ is the sand ratio of SFRMC; $\beta_{s,0}$ is the sand ratio of referenced mixed-sand concrete; η_f is the fiber factor, which is the product of the aspect ratio multiplied by the volume fraction of steel fiber and considered the influence of the fiber form; and α_f is the coefficient of the fiber form, with $\alpha_f = 0.90$ for ingot mill steel fibers.

Table 3 presents the results of the mix proportions of SFRMC. On the premise of equivalent activity indices of mineral admixtures in this study [42], the content of silica fume was 6%, 8%, and 10%, respectively, corresponding to β_{fa} of 45%, 60%, and 75%. For the ID of mixes, the letter F followed by a number represents the percentage content of fly ash: 30%, 45%, 60%, or 75%; the letter SF followed by a number represents the volume fraction of steel fibers: 0%, 0.4%, 0.8%, 1.2%, or 1.6%.

Table 3. Dosages of raw materials and tested wet and dry unit weights of SFRMC (kg/m^3).

ID	Cement	Fly Ash	Silica Fume	Water	SRS	MS	Crushed Limestone	Steel Fiber	Water Reducer	Unit Weight	
										Wet	Dry
F30	335.4	143.7	-	172.5	335.9	503.9	909.7	0	3.35	2415	2266
F30SF4	347.4	148.9	-	178.6	318.4	477.6	910.4	31.4	3.47	2410	2300
F30SF8	358.3	153.6	-	184.2	322.1	483.1	859.5	62.8	3.58	2450	2310
F30SF12	369.2	158.2	-	189.9	325.7	488.5	808.9	94.2	3.69	2470	2320
F30SF16	380.2	162.9	-	195.5	329.2	493.9	758.4	125.6	3.80	2490	2340
F45SF8	250.8	230.3	30.7	184.2	313.5	470.2	834.9	62.8	3.58	2390	2300
F60SF8	163.8	307.1	40.9	184.2	308.2	462.4	820.0	62.8	3.58	2340	2210
F75SF8	76.8	383.9	51.2	184.2	305.0	454.5	805.0	62.8	3.58	2330	2190

For the mix proportion design of SFRMC, the aggregates were assumed to be in a surface-dry saturated condition. Therefore, the additional water required should be computed by subtracting the water content of the aggregates from their water absorption. Using a horizontal shaft forced mixer, the crushed limestone, manufactured sand, and SRS were first added and soaked with the additional water for 30 s. The steel fibers were then added and mixed for 20 s, followed by the addition of the binders and another 30 s of mixing. Finally, the mixing water and water reducer were added and mixed for 2 min.

The workability of the fresh mix was tested, and the test specimens were formed in a room maintained at a temperature of (20 ± 5) °C and a relative humidity above 45%. Subsequently, the specimens were cured in a standard curing room at a temperature of (20 ± 2) °C and a relative humidity of no less than 95%.

2.3. Test Methods

After the cubic specimens were formed and cured for 28 days, the wet and dry unit weights of SFRMC were tested according to China code GB 50080 [43]. The results are summarized in Table 3. The unit weight of SFRMC increased with the volume fraction of steel fibers, as the steel fibers have a higher density than the other constituents. A strong correlation was observed between tested and designed wet unit weights, with ratios ranging from 0.994 to 1.016. This indicates that the absolute volume method is a reasonable approach for the mix proportion design of SFRMC. In general, the dry unit weight was between 91.2% and 96.2% of the wet unit weight, indicating a loss of free water amounting to 3.8–8.8% of the wet unit weight during the concrete hardening process.

The workability of the fresh mix was determined in accordance with the specifications of China code GB/T 50080 [43]. The tests conducted included the slump and slump flow, the static segregation rate, the pressure bleeding rate, and the air content. The rheological properties of the fresh mixture, including the yield stress and plastic viscosity, were measured using the eBT-V concrete rheometer produced by Gemany Schleibinger Co., Ltd., Buchbach, Germany [20].

The water absorption at a curing age of 28 days and mechanical properties of SFRMC were tested as per China code GB/T 50081 [44]. Standard specimens were prepared for

testing. Two hours before testing, the specimens were moved out of the curing room. The surfaces of the specimens were dried with a soft cloth. The water absorption was measured using a cubic specimen with dimensions of 100 mm. The cubic compressive strength and the splitting tensile strength were tested using a cubic specimen with dimensions of 150 mm. The axial compressive strength and the modulus of elasticity were tested using a prismatic specimen of 150 mm × 150 mm × 300 mm. The flexural toughness was measured using a beam specimen of 150 mm × 150 mm × 550 mm, with a span of 450 mm, by the four-point loading test. For each kind of test, three specimens were tested per trial. As the normal content of fly ash has some influence on the strength development of concrete [20,21,33], all the mechanical properties were measured at the curing age of 28 days for the SFRMC with varying volume fractions of steel fibers. Meanwhile, considering that the concrete with a high content of fly ash has a lower strength at an early age but better long-term strength [21,31], the mechanical properties were measured at a curing age of 90 days for SFRMC with varying fly ash contents.

3. Discussion on Workability

The test results of the workability and the rheological properties of fresh mixes are summarized in Table 4. A discussion of test results affected by the experimental parameters is given below.

Table 4. Test results of the workability and rheological properties of fresh mixes.

ID	Workability							Rheological Properties	
	S(mm)			SF (mm)	Air Content (%)	Static Segregation Rate (%)	Pressure Bleeding Rate (%)	τ_0 (Pa)	η_0 (Pa·s)
	Initial	0.5 h	1 h						
F30SF4	220	190	175	390	4.1	0.20	38.7	24.6	14.1
F30SF8	215	175	155	380	4.7	0.30	35.1	45.3	24.9
F30SF12	215	170	150	450	4.9	1.00	32.1	80.6	44.0
F30SF16	225	165	125	470	4.8	2.20	30.0	101.7	55.5
F45SF8	205	-	150	350	2.8	0.20	30.8	60.6	15.4
F60SF8	215	-	150	360	4.6	0.20	20.6	77.1	17.0
F75SF8	210	-	140	330	3.8	0.20	18.8	93.8	17.7

3.1. Slump Flowability

Figure 1 presents the slump flowability and rheological properties of fresh SFRMC with varying volume fractions of steel fibers. In general, the initial slump basically remained constant, while the initial slump flow increased with the volume fraction of steel fibers. Contrary to normal expectations, the slump flow increased with the fiber content. This is due to the adjustment of the mix proportion of SFRMC with an increased water dosage and sand ratio computed with Formulas (1) and (2). To keep a consistent water-to-binder ratio, the content of binders increased with the water dosage, which increased the binder paste wrapping around the steel fibers and aggregates. The increase in the sand ratio increased the mortar volume to improve the filling ability in the gaps of coarse aggregates, which directly reduced the confinement on the flow of the fresh mix. All of these factors led to an increase in the lubrication action of mortar, which minimized the flow friction among the interfaces of aggregate particles. However, because a large volume of binder paste was dispersed and wrapped around the superfine grains of SRS with a much larger specific surface area, the residual binder paste was not enough to wrap around the surfaces of steel fibers [35,42,45]. The flowability of fresh SFRMC could not increase as expected.
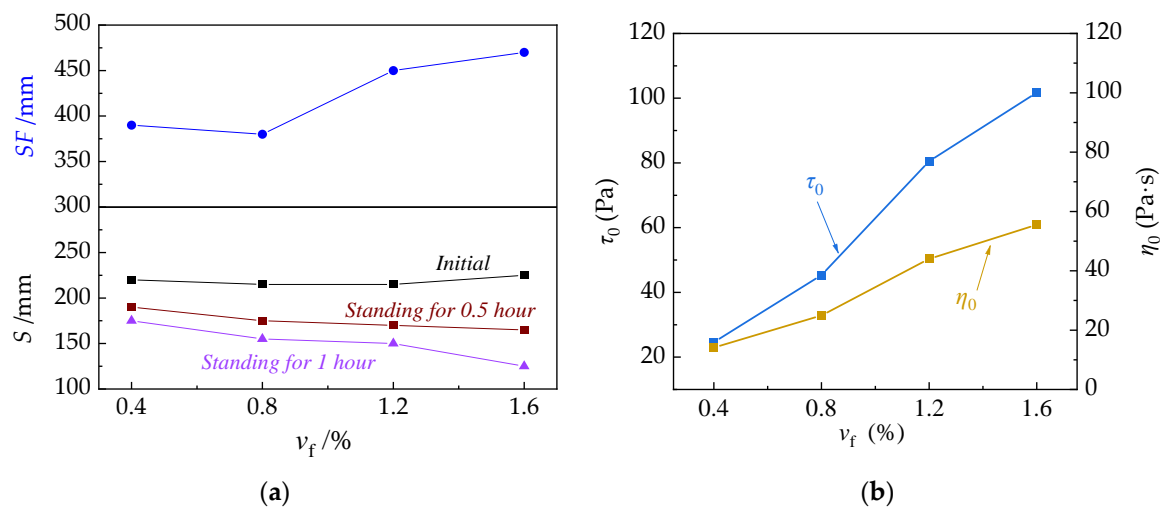
Figure 1. Slump flowability and rheological properties of fresh SFRMC with varying volume fractions of steel fiber: (**a**) flowability; (**b**) rheological properties.

Influenced by the coupling of steel fibers and mixed-sand mortar, the relationship between the slump flowability and the rheological properties was opposite to the theoretical prediction. The need for binder paste wrapped around steel fibers and the amount of mortar filling the gaps between aggregates should be coordinated to obtain adequate flowability of fresh SFRMC. Although the needle-like adhesion of steel fibers increases the plastic tension, which resists the collapse of fresh SFRMC, the flowability of fresh SFRMC increased due to static segregation. The effect of steel fibers on the rheological properties of fresh SFRMC was reflected in the slump loss, which caused the increase in the slump loss of fresh SFRMC with the volume fraction of steel fibers after standing for 1 h. However, although a higher slump loss existed for fresh SFRMC after standing for 1 h, the slump could be regained by vibration [34,36]. In this condition, the needle-like adhesion of steel fibers to the SFRMC matrix can be broken with vibrations.

3.2. Static Segregation Rate, Pressure Bleeding Rate, and Air Content

As shown in Table 4, the static segregation rate, which is the mass percent of segregated binder paste relative to the fresh mix at static standing, was 0.2–2.2%. It had a tendency to increase with the volume fraction of steel fibers. This is because the water dosage and the sand ratio increased with the volume fraction of steel fibers in the mix proportion design in this study. Abundant binder paste can more easily segregate without bonding to aggregates. However, this is not an issue, as the values were far below the limitation of 10% specified in China code JGJ/T 283 [46].

The pressure bleeding rate, which is the mass ratio of bleeding water from fresh concrete under pressure for 10 s to that under pressure for 140 s, decreased with the increase in the volume fraction of steel fibers. This indicates that the increase in the water dosage is rational for the volume fraction of steel fibers. However, the SFRMC had a larger bleeding rate when the volume fraction of steel fibers was 0.4%. Generally, the pressure bleeding rate is lower than the limit of 40% specified in China code JGJ/T 10 [47]. This is to ensure better compaction quality of fresh SFRMC without surficial bleeding watermarks in engineering applications.

From the test results presented in Table 4, it can be seen that the air content in fresh mixes tended to increase with the volume fraction of steel fibers. This indicates that the steel fibers oriented in fresh mixes can provide channels for air entraining into the gaps of aggregates. The experimental air content was 2.8–4.9%, which meets the requirement to be less than 5.5% specified by Chinese code GB 50164 [12]. This is beneficial for eliminating pits with air bubbles on the surface of compacted fresh SFRMC.

4. Analyses of Mechanical Properties

Tables 5 and 6 summarize the test results of SFRMC, including the cubic compressive strength (f_{cu}), the axial compressive strength (f_c), the modulus of elasticity (E_c), the splitting tensile strength (f_{st}), the flexural strength (f_f), and the water absorption. The failure patterns of SFRMC specimens under compression, splitting and bending were similar to those of conventional SFRC under the same conditions [34,36]. No special features appeared on the SFRMC specimens. That is, the brittleness of SFRMC turned to plasticity with the increase in the volume fraction of steel fiber due to the steel-fiber bridge across the main crack, which kept the integrity of specimens, while some secondary cracks appeared on specimens with a higher volume fraction, over 1.2%, of steel fibers. The standard variation in cubic compressive strength is 1.7–2.6 MPa, which is lower than 3.5 MPa for the concrete at strength grade C40 (corresponding to a target compressive strength of 48.2 MPa) specified in China code GB50164 [12]. The standard variation in axial compressive, splitting tensile, and flexural strengths is 0.67–1.22 MPa, 0.12–0.19 MPa, and 0.11–0.16 MPa, respectively. The standard variation in the modulus of elasticity is 0.46–1.14 GPa. The standard variation in water absorption is 0.17%.

Table 5. Test results of SFRMC with varying steel fiber contents at curing age of 28 days.

ID	Water Absorption (%)	f_{cu} (MPa)	f_c (MPa)	E_c (GPa)	f_{st} (MPa)	f_f (MPa)
F30	4.0	48.9	40.9	33.1	3.49	4.2
F30SF4	4.4	48.7	39.2	34.2	3.60	4.8
F30SF8	4.6	49.2	40.5	36.7	3.84	5.0
F30SF12	5.3	48.8	39.9	37.4	3.94	5.8
F30SF16	5.4	54.1	43.9	39.5	4.28	6.1

Table 6. Test results of SFRMC with varying fly ash contents at curing age of 90 days.

ID	Water Absorption (%)	f_{cu} (MPa)	f_c (MPa)	E_c (GPa)	f_{st} (MPa)	f_f (MPa)
F30SF8	4.4	55.8	45.7	36.8	3.96	-
F45SF8	4.1	66.0	53.0	37.4	4.11	4.2
F60SF8	4.0	49.1	38.1	32.2	2.95	4.1
F75SF8	4.5	22.7	18.3	20.5	1.65	3.5

The water absorption reflects the porosity and the casting quality of the hardened SFRMC. A lower water absorption indicates a dense structure of hardened SFRMC with a high compaction quality. As shown in Table 5, the increase in steel fiber content led to an increase in water absorption from 4.0% to 5.4%. This indicates that the steel fibers could connect the pores of hardened SFRMC. As shown in Table 6, the water absorption tended to decrease with the increase in fly ash content, while that of SFRMC with 75% fly ash content went back to a higher value of 4.5%. Generally, the water absorption was at a low level, which indicates good compaction.

4.1. Compressive Properties

The cubic compressive strength of SFRMC varied from 48.7 MPa to 54.1 MPa, as shown in Table 5. No obvious tendencies appeared as the volume fraction of steel fiber increased from 0.4% to 1.2%, while an increment of about 11% in the cubic compressive strength of SFRMC was observed with a volume fraction of steel fiber of 1.6%. This is basically consistent with other studies on conventional SFRC reporting that the cubic compressive strength was slightly influenced by a volume fraction of steel fibers of 0.4–2.0% [34,35]. This is attributed to the lower transversal deformation of cubic specimens under compression, which is provided by the restriction of steel fibers. In this study, the cubic compressive

strength of SFRMC was over the target value of 48.2 MPa. This once again demonstrated the reasonability of using the mix design method for SFRMC.

By analyzing the test data listed in Table 5, a similar variation with the volume fraction of steel fiber was observed in the axial compressive strength and cubic compressive strength of SFRMC. This is consistent with the similar loading process of specimens under compression. Because the transversal deformation of prismatic specimens is larger than that of cubic specimens, the axial compressive strength is lower than the cubic compressive strength. According to China code GB 50010 [26], the relationship between axial compressive strength and cubic compressive strength is $f_c = 0.76 f_{cu}$. With the stronger confinement of steel fibers to the transversal deformation of a prismatic specimen, the ratio of experimental f_c/f_{cu} of SFRMC at a curing age of 28 days varied from 0.805 to 0.823, with an average of 0.814 and a deviation coefficient of 0.009. The results were all over 0.76, which indicates that the SFRMC can be safely applied under compression.

As specified in China code GB 50010 [26], the modulus of elasticity of conventional concrete can be determined by the following equation:

$$E_c = \frac{10^5}{2.2 + 34.7/f_{cu}} \tag{4}$$

The ratio between the experimental and predicted results decreased from 1.038 to 0.764 for SFRMC with 30–75% fly ash content at a curing age of 90 days. This indicates that the modulus of elasticity of SFRMC with a fly ash content of less than 60% was similar to that of conventional concrete. The modulus of elasticity of SFRMC with 75% fly ash content was lower due to the insufficient hydration of cement and the lack of secondary hydration of fly ash and silica fume. In general, Equation (4) can be used for predicting the modulus of elasticity for SFRMC with a fly ash content of less than 60%.

As shown in Figure 2, the modulus of elasticity of SFRMC with 30% fly ash content linearly increased with the steel fiber factor, which indicates that the confinement of steel fibers to the transverse deformation of a prismatic specimen can improve the modulus of elasticity of SFRMC under axial compression. However, the positive relationship did not appear for the modulus of elasticity of conventional SFRC [34,35]. This is a point of future study that should be verified for the compressive performance of SFRMC.
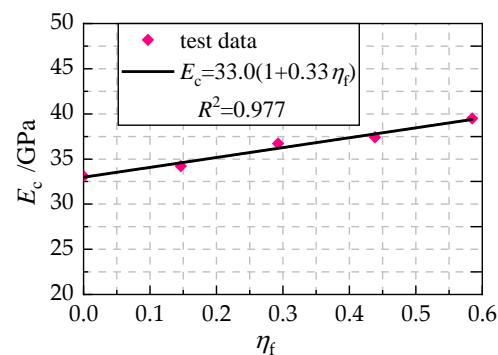

Figure 2. Modulus of elasticity of SFRMC changed with steel fiber factor.

Because the dosage of cement decreased with the increase in fly ash content, the cement hydrates decreased in quantity, which weakened the strength formation of SFRMC at an early age. However, with the increase in curing age, the fly ash and silica fume played a role in secondary hydration with byproducts of cement hydrates [33,42]. This improves the strength development of SFRMC in the long term. As shown in Table 6, SFRMC still shows a decreasing tendency of cubic compressive strength at a curing age of 90 days with the increase in fly ash content. Even so, SFRMC with fly ash content of less than 60% could reach, or even exceed, the target cubic compressive strength of 48.2 MPa.

4.2. Splitting Tensile Strength

As shown by the test results listed in Table 5, the splitting tensile strength of SFRMC increased with the volume fraction of steel fibers. This is in line with studies on high-flowability SFRC [34,35]. Because the bonding of steel fibers with concrete matrix forms a bridge effect, acting as micro-reinforcements across the splitting section, an interlocking structure is built from the coarse aggregates and the steel fibers. From this aspect, the stability of the interlocking structure can be enhanced with a larger volume fraction of steel fibers. As presented in Figure 3, the splitting tensile strength f_{st} of SFRMC can be predicted as:

$$f_{st} = 3.45(1 + 0.38\eta_f) \tag{5}$$
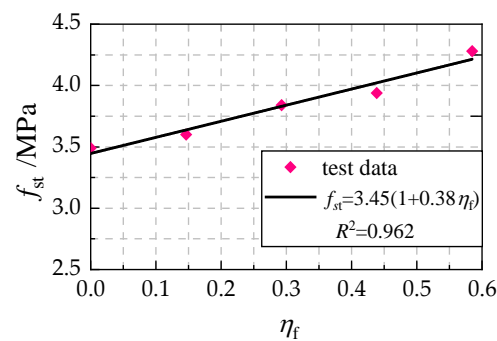
Figure 3. Splitting tensile strength of SFRMC changed with steel fiber factor.

The f_{st} of SFRMC with 45% fly ash content at a curing age of 90 days was over the limitation specified in the code, while the f_{st} of SFRMC with 60% fly ash content was less than that of SFRMC with 30% fly ash content.

4.3. Flexural Performance

Figure 4 presents the linear fit of the flexural strength of SFRMC with the steel fiber factor, and it is expressed as:

$$f_f = f_{f0}(1 + 0.78\eta_f) \tag{6}$$

where f_{f0} is the flexural strength of reference mixed-sand concrete without steel fibers.
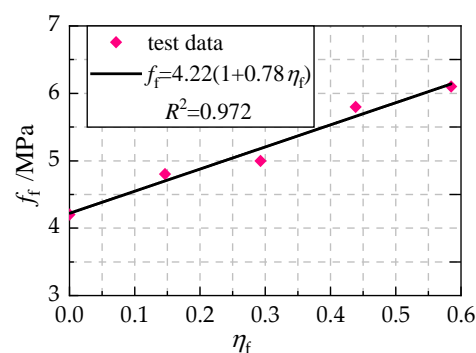

Figure 4. Flexural strength of SFRMC changed with steel fiber factor.

Equation (6) is familiar to us due to the micro-reinforcement effect of steel fibers in the concrete matrix, which resists cracking and bridges cracks so that tensile stress is transferred from the cracked concrete matrix. The reinforcing contribution of steel fibers to the flexural strength is higher than that of the splitting tensile strength. This is attributed to the different distribution and orientation of steel fibers in cubic specimens and beam specimens [34,35]. With the high-flowing workability of SFRMC, steel fibers tended to distribute along the longitudinal direction of beam specimens, which is consistent with the main direction of flexural tensile stress, which provides a higher reinforcement of bending sections to resist the flexural moment.

The complete load–deflection curves of the test beam specimens with varying volume fractions of steel fibers are shown in Figure 5. Each curve represents a group of three test beam specimens and was obtained by generating the load–deflection curves of a group, similar to dealing with a group of load–bond-slip curves [39]. With the increase in the volume fraction of steel fibers from 0.4% to 1.6%, the load–deflection curve became fuller with a higher residual loading capacity. This is attributed to the steel fibers bridging cracks and absorbing the tensile stress released from the cracked concrete matrix [35,36]. Meanwhile, when the volume fraction of steel fiber was over 1.2%, a second peak load appeared after the first peak load. This indicates that the first peak load can be absorbed by the steel fibers across the main crack, and a higher load can be reached due to the rebalance of sectional stresses. By observing the broken sections of tested beam specimens, the number of steel fibers counted across the section was 64, 93, 114, and 142, respectively, corresponding to volume fractions of steel fibers of 0.4%, 0.8%, 1.2%, and 1.6%. This provides a condition in which crack elongation along the cracked section was postponed by the presence of many more steel fibers, which led to a high flexural stiffness resisting deformation [36].
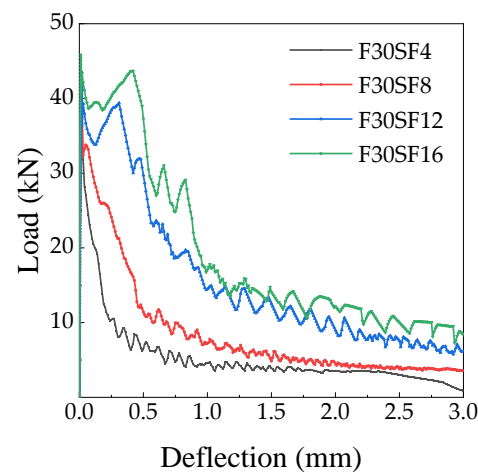

Figure 5. Tested load–deformation curves of SFRMC beam specimens with different volume fractions of steel fibers.

The opening of the crack width leads to a larger bond slip of steel fibers with the concrete matrix. With the loss of bonding between steel fibers and concrete matrix, the steel fibers are continuously pulled out of the cracked section, and the reinforcement effect of steel fibers becomes weak [39]. The load decreases when the concrete matrix starts cracking and increases with the following reinforcement action of steel fibers. This makes the load–deflection curves present a zigzag shape in the descending portion. When some of the steel fibers lost the bond with the concrete matrix or broke in the cracked section, the deformation presented a sharp increment with a rapid drop in the load.

The complete load–deflection curves of test beam specimens with varying fly ash contents are shown in Figure 6. A second peak load is observed after the first peak load for SFRMC with 45% and 60% contents of fly ash, while the peak load directly appears with a larger deflection for SFRMC with 75% content of fly ash. This is an interesting phenomenon. Although the corresponding peak load decreases, the descending part of the load–deflection curve becomes fuller with increases in fly ash content, especially at 75% fly ash content.

The flexural toughness of SFRC was computed as per China code JG/T 472 [40]. The pre-peak-load–deflection toughness is expressed by the initial flexural toughness ratio $R_{e,p}$, where a larger $R_{e,p}$ indicates a better enhancement of the flexural performance of SFRC before it reaches the ultimate flexural strength. The post-peak-load–deflection toughness in an l_0/k (l_0 is the span of test beam specimens, k = 500, 300, 250, 200, 150) condition is

represented by the remaining flexural toughness ratio $R_{e,k}$, where a larger $R_{e,k}$ indicates that steel fibers make a greater contribution to the remaining flexural strength and energy absorption capability of SFRC [35,36].
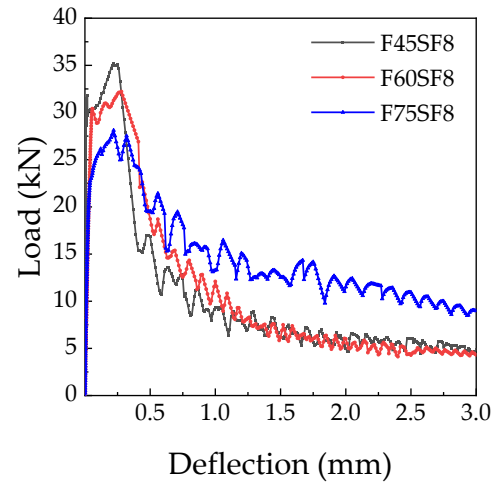

Figure 6. Tested load–deflection curves of SFRMC beam specimens with varying fly ash contents.

The results of the flexural toughness of SFRMC changed with the steel fiber factor and the fly ash content, as shown in Figure 7. This indicates that the flexural toughness of SFRMC increases with the increase in the volume fraction of steel fibers and the fly ash content.
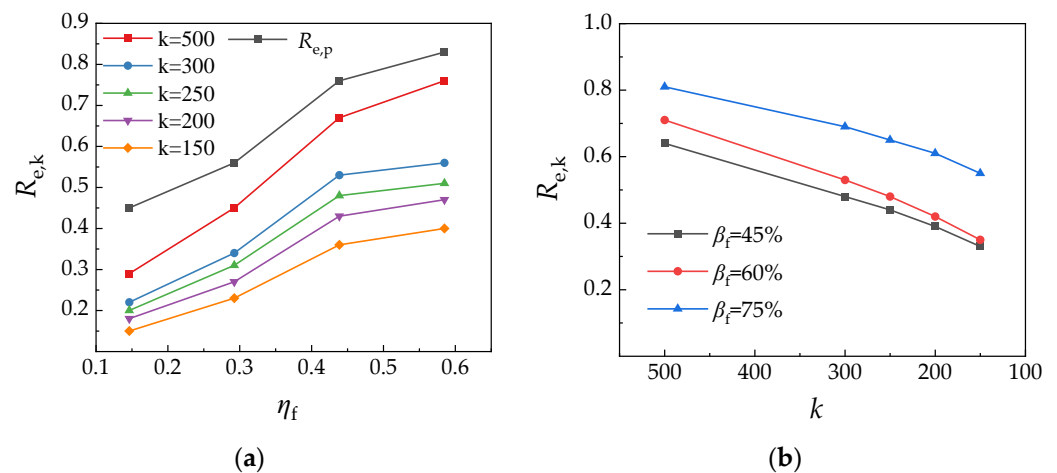

(**a**)

(**b**)

Figure 7. Flexural toughness ratio of SFRMC with varying contents of (**a**) steel fibers; (**b**) fly ash.

5. Conclusions

In this study, the workability and mechanical properties of high-flowability steel-fiber-reinforced concrete (SFRMC) were experimentally studied. Mixed sand was combined with superfine river sand and coarse manufactured sand, and a high content of fly ash was used with silica fume under the condition of the equivalent activities of blended admixtures with fly ash and silica fume. The conclusions can be summarized as follows.

The absolute volume method was adaptable to the design of SFRMC considering the influence of steel fibers, in which the water dosage and the sand ratio were adjusted with the fiber content to ensure the reasonable workability of the fresh mix. Fresh mixes with a slump of (220 ± 5) mm could be prepared, while the static segregation rate, pressure bleeding rate, and air content were all within the limits.

Both the cubic compressive strength and axial compressive strength of SFRMC were slightly influenced by the presence of steel fibers, while the modulus of elasticity presented

an increasing tendency with the increase in steel fiber content. The tensile strength and flexural strength of SFRMC were significantly reinforced with the steel fibers and increased linearly with the fiber factor, with reinforcing coefficients of 0.38 and 0.78, respectively. When the volume fraction of steel fibers was over 1.2%, a second peak load appeared after the first peak load in the complete load–deflection curve of SFRMC. This obviously contributed to the increase in the flexural toughness of SFRMC. The remaining flexural toughness kept increasing, although the flexural strength of SFRMC decreased with the increase in fly ash content.

The study in this paper only considered one proportion of SRS with manufactured sand to compose the mixed sand, with SFRMC at a strength grade of C40. To ensure the construction quality of SFRMC for wide engineering applications, further studies should be continuously conducted to evaluate how the performance of fresh and hardened SFRMC is influenced by mixed sand and fly ash.

Author Contributions: Conceptualization and methodology, C.L., Y.Z. and F.L.; investigation, H.G., H.W. and H.Z.; writing—original draft preparation, H.G., H.W. and H.Z.; writing—review and editing, C.L. and Y.Z.; funding acquisition, C.L. and Y.Z.; supervision, F.L. All authors have read and agreed to the published version of the manuscript.

Data Availability Statement: Data are available from the first author and can be shared with anyone upon reasonable request.

Conflicts of Interest: The authors declare no conflict of interest.

References

1. *JGJ/T 240-2011*; Technical Specification for Application of Recycled Aggregate. China Building Industry Press: Beijing, China, 2011.
2. Tanol, T.; Ömer, D.; Salahi, P. Influences of recycled plastic and treated wastewater containing with 50% GGBS content in sustainable concrete mixes. *J. Mater. Res. Technol.* **2022**, *16*, 110–128. [CrossRef]
3. *GB/T 51003-2014*; Technical Code for Application of Mineral Admixtures. China Building Industry Press: Beijing, China, 2014.
4. Xuan, M.; Wang, X. Effect of belite-rich cement replacement on the properties enhancement of eco-friendly ultra-high performance concrete containing limestone powder and slag. *J. Mater. Res. Technol.* **2023**, *23*, 1487–1502. [CrossRef]
5. *JGJ/T 241-2011*; Technical Specification for Application of Manufactured Sand Concrete. China Building Industry Press: Beijing, China, 2011.
6. *JGJ/T361-2014*; Technical Specification for Application of Crushed Gravel Mixed-Sand. China Building Industry Press: Beijing, China, 2014.
7. Zhao, S.; Han, B.; Ding, X. Study on properties of manufactured sand and its concrete by our research group. In *3rd International Conference on Civil Engineering, Architecture and Sustainable Infrastructure*; DEStech Publications, Inc.: Lancaster, PN, USA, 2015; pp. 16–21.
8. Shen, W.; Yang, Z.; Cao, L.; Cao, L.; Liu, Y.; Yang, H.; Lu, Z.; Bai, J. Characterization of manufactured sand: Particle shape, surface texture and behavior in concrete. *Constr. Build. Mater.* **2016**, *114*, 595–601. [CrossRef]
9. Ufuk, D. Effects of manufactured sand characteristics on water demand of mortar and concrete mixtures. *J. Test. Eval.* **2015**, *43*, 562–673.
10. Huang, Y.; Wang, L. Effect of particle shape of limestone manufactured sand and natural sand on concrete. *Procedia Eng.* **2017**, *210*, 87–92.
11. Sara, C.; Franco, M. Assessing the quality control of self-consolidating concrete properties. *J. Constr. Eng. Manag.* **2012**, *138*, 197–205.
12. *GB 50164-2011*; Standard of Quality Control for Concrete. China Building Industry Press: Beijing, China, 2011.
13. Xu, W.K.; Chen, S.L.; Li, P.; Gu, G.C. Distribution characteristics of sedimentation and suspended load and their indications for erosion-siltation in the littoral of Yellow River delta. *J. Sediment. Res.* **2016**, *3*, 24–30.
14. Li, C.; Song, L.; Cao, Y.; Zhao, S.; Liu, H.; Yang, C. Investigating the mechanical property and enhanced mechanism of modified Pisha sandstone geopolymer via ion exchange solidification. *Gels* **2022**, *8*, 300. [CrossRef]
15. Luan, J.; Chen, X.; Ning, Y.; Shi, Z. Beneficial utilization of ultra-fine dredged sand from Yangtze River channel as a concrete material based on the minimum paste theory. *Case Studies Constr. Mater.* **2022**, *16*, e01098. [CrossRef]
16. Wang, F.; Lu, J.; Zhao, S.; Shi, Z.; Liu, J. Experimental study on the superfine sand modified manufactured sand to prepare C60 concrete. *New Build. Mater.* **2022**, *49*, 22–27.
17. Wang, L.X. Application of Yellow River sand in high flowing concrete. *Yellow River* **2017**, *39*, 106–111.

18. Shang, P.; Wang, H.; Zhang, D.; Zheng, W.; Qu, F.; Zhao, S. Experimental study on external loading performance of large diameter prestressed concrete cylinder pipe. *Buildings* **2022**, *12*, 1740. [CrossRef]
19. Yang, Y.; Ding, X.; Liu, Y.; Deng, L.; Lv, F.; Zhao, S. Lateral pressure test of vertical joint concrete and formwork optimization design for monolithic precast concrete structure. *Buildings* **2022**, *12*, 261. [CrossRef]
20. Zhao, M.; Dai, M.; Li, J.; Li, C. Case study on pumpability and mechanical property of concrete with manufactured sand and super-fine river sand. *Case Study Constr. Mater.* **2023**, *18*, e01850.
21. Li, C.; Geng, H.; Zhou, S.; Dai, M.; Sun, B.; Li, F. Experimental study on preparation and performance of concrete with large content of fly-ash. *Front Mater.* **2022**, *8*, 764820. [CrossRef]
22. Matos, P.R.; Foiato, M.; Prudêncio, L.R., Jr. Ecological, fresh state and long-term mechanical properties of high-volume fly ash high-performance self-compacting concrete. *Constr. Build. Mater.* **2019**, *203*, 282–293. [CrossRef]
23. *JGJ 55-2011*; Specification for Mix Proportion Design of Ordinary Concrete. China Building Industry Press: Beijing, China, 2011.
24. *GB/T 50146-2014*; Technique Code for Application of Fly Ash Concrete. China Standard Press: Beijing, China, 2014.
25. *JGJ 52-2006*; Standard for Technical Requirements and Test Method of Sand and Crushed Stone (or Gravel) for Ordinary Concrete. China Building Industry Press: Beijing, China, 2006.
26. *GB 50010-2010*; Code for Design of Concrete Structures. China Building Industry Press: Beijing, China, 2010.
27. Herath, C.; Gunasekara, C.; Law, D.W.; Setunge, S. Performance of high volume fly ash concrete incorporating additives: A systematic literature review. *Constr. Build. Mater.* **2020**, *258*, 120606. [CrossRef]
28. Hosan, A.; Shaikh, F.U.A. Compressive strength development and durability properties of high volume slag and slag-fly ash blended concretes containing nano-CaCO$_3$. *J. Mater. Res. Technol.* **2021**, *10*, 1310–1322. [CrossRef]
29. Promsawat, P.; Chatveera, B.; Suaiam, G.; Makul, N. Properties of self-compacting concrete prepared with ternary Portland cement-high volume fly ash-calcium carbonate blends. *Case Study Constr. Mater.* **2020**, *13*, e00426. [CrossRef]
30. Nežerka, V.; Bílý, P.; Hrbek, V.; Fládr, J. Impact of silica fume, fly ash, and metakaolin on the thickness and strength of the ITZ in concrete. *Cem. Concr. Compos.* **2019**, *103*, 252–262. [CrossRef]
31. Park, B.; Choi, Y.C. Hydration and pore-structure characteristics of high-content fly ash cement pastes. *Constr. Build. Mater.* **2021**, *278*, 122390. [CrossRef]
32. Choi, Y.W.; Park, M.S.; Choi, B.K.; Oh, S.R. A study on the evaluation of field application of high-fluidity concrete containing high volume fly ash. *Adv. Mater. Sci. Eng.* **2015**, *2015*, 507018. [CrossRef]
33. Yu, J.; Lu, C.; Leung, C.K.Y.; Li, G.Y. Mechanical properties of green structural concrete with ultrahigh-volume fly ash. *Constr. Build. Mater.* **2017**, *147*, 510–518. [CrossRef]
34. Ding, X.; Li, C.; Han, B.; Lu, Y.; Zhao, S. Effects of different deformed steel-fibers on preparation and fundamental properties of self-compacting SFRC. *Constr. Build. Mater.* **2018**, *168*, 471–481. [CrossRef]
35. Zhao, M.; Li, J.; Xie, Y.M. Effect of vibration time on steel fibre distribution and flexural properties of steel fibre reinforced concrete with different flowability. *Case Study Constr. Mater.* **2022**, *16*, e01114.
36. Zhao, M.; Li, J.; Law, D. Effects of flowability on SFRC fibre distribution and properties. *Mag. Concr. Res.* **2017**, *69*, 1043–1054. [CrossRef]
37. Iqbal Khan, M.; Abbass, W.; Alrubaidi, M.; Alqahtani, F.K. Optimization of the fine to coarse aggregate ratio for the workability and mechanical properties of high strength steel fiber reinforced concretes. *Materials* **2020**, *13*, 5202. [CrossRef]
38. Ding, X.; Zhao, M.; Li, J.; Shang, P.; Li, C. Mix proportion design of self-compacting SFRC with manufactured sand based on the steel fiber-aggregates skeleton packing test. *Materials* **2020**, *13*, 2833. [CrossRef]
39. Ding, X.; Zhao, M.; Li, C.; Li, J.; Zhao, X. A multi-index synthetical evaluation of bond behaviors of hooked-end steel fiber embedded in mortars. *Constr. Build. Mater.* **2021**, *276*, 122219. [CrossRef]
40. *JG/T 472-2015*; Steel Fiber Reinforced Concrete. China Standard Press: Beijing, China, 2015.
41. *GB/T 27690-2011*; Silica Fume for Mortar and Concrete. China Standard Press: Beijing, China, 2011.
42. Liu, S.; Zhu, M.; Ding, X.; Ren, Z.; Zhao, S.; Zhao, M.; Dang, J. High-durability concrete with supplementary cementitious admixtures used in corrosive environments. *Crystals* **2021**, *11*, 196. [CrossRef]
43. *GB/T 50080-2016*; Standard for Test Method of Fresh Performance of Ordinary Concrete. China Building Industry Press: Beijing, China, 2016.
44. *GB/T 50081-2019*; Standard for Test Method of Physical and Mechanical Properties of Concrete. China Building Industry Press: Beijing, China, 2019.
45. Rama, J.S.K.; Sivakumar, M.V.N.; Kubair, K.S.; Vasan, A. Influence of plastic viscosity of mix on self-compacting concrete with river and crushed sand. *Comput. Concr.* **2019**, *23*, 37–47.
46. *JGJ/T 283-2012*; Technical Specification for Application of Self-compacting Concrete. China Building Industry Press: Beijing, China, 2012.
47. *JGJ/T 10-2011*; Technical Specification for Construction of Concrete Pumping. China Building Industry Press: Beijing, China, 2011.